Improving the Estimation of the Wavenumber Spectra From Altimeter Observations

Corinne Mailhes, *Member, IEEE*, Olivier Besson, Amandine Guillot, and Sophie Le Gac

***Abstract*— Satellite altimeters provide sea-level measurements along satellite track. A mean profile based on the measurements averaged over a time period is then subtracted to estimate the sea-level anomaly (SLA). In the spectral domain, SLA is characterized by a power spectral density (PSD) whose slope in a log–log scale is a parameter of great interest for ocean monitoring. Estimation of this spectral slope is usually done through a cumulated periodogram using a large number of signal samples. The location and dates of the data induce the spatial and temporal resolution of the slope estimates. To improve this resolution, this article studies a new parametric method based on an autoregressive model combined with a warping of the frequency scale (denoted as ARWARP). This ARWARP model provides a PSD estimate, with a lower variance than the classical Fourier-based ones and is reliable in the case of a small sample number. To give a reference in the performance of the SLA slope estimation, the corresponding Cramér–Rao bound is derived. Then, rather than performing linear regression on the spectral estimates, a new estimator of the slope is suggested, based on a model fitting of the PSD. A statistical validation is proposed on simulated SLA signals, showing the performance of slope estimation using this ARWARP spectral estimator, compared to classical Fourier-based methods. Application to Sentinel-3 real data highlights the main advantage of the ARWARP model, making possible SLA slope estimation on a short signal segment, i.e., with a high spatial and/or temporal resolution.**

***Index Terms*— Autoregressive (AR) model, frequency warping, sea-level anomaly (SLA), slope estimation, spectral analysis.**

I. Introduction

THE history of satellite altimetry began in the 1970s, but the performance of this technique improved considerably in the 1990s with Topex/POSEIDON. This revolutionized the scientific knowledge on sea-level variations, at regional and global scales [1]. Topex/POSEIDON was the first item of the Jason series (Jason-1 operating from 2001 to 2013, Jason-2 from 2008 to 2019, Jason-3 from 2016, and Jason-CS/Sentinel-6 launched in 2020), considered as the reference mission for mean sea-level monitoring [2]. The Sentinel-3 topography mission (European Commission Copernicus Program) aims at complement these reference time series for operational applications and mesoscale monitoring. Satellites A and B are currently in-flight (respectively, launched in 2016 and 2018), and the continuity will be ensured with C and D items [3].

Actually, satellite altimetry is used for a wide range of applications. Over ocean, the measured data benefit, for example, to meteorological applications, by measuring the surface wind speed and the significant wave height [4]. Satellite altimetry is also commonly used over hydrology, i.e., to monitor rivers and lakes elevation [5]. The added value of satellite with respect to *in situ* means is the global coverage, repeated in time. The height variations measured can be then used to estimate the fresh water fluxes and resources. Another major field of application for altimetry is the cryosphere monitoring (obviously with a proper orbit coverage), which mostly corresponds to ice sheet elevation and sea ice thickness monitoring [6]. This topic is strongly related to issues in climate change, as the mass loss of ice sheet is the main contributor of sea-level rise, and sea ice loss and thinning represents at the same time an evidence of climate change and an amplification factor (albedo effect). However, the main goal of most altimetry missions (such as Sentinel-3) is to monitor sea-level variations.

As such, satellite altimetry has strongly contributed to reveal that the circulation is dominated by mesoscale variability, due to ocean eddies or isolated vortices, meandering currents or fronts, squirts, and filaments. The mesoscale variability usually refers to ocean signals with space scales of around 100 km. The mesoscale can be observed thanks to the sea-level anomaly (SLA) variable, which is deduced from the measured sea level minus a mean level computed by averaging a long time series of sea-level data [7].

The estimation of the wavenumber spectra of along-track SLA is a relevant way to evidence energy cascades between large-scale (≈1000 km), mesoscale (≈100 km), and submesoscale (few tens kilometers) dynamics [8]. In such a representation, geostrophic mesoscale turbulence appears as a steep slope in the mesoscale wavelength band. The slope value (denoted by α thereafter) exhibits spatial variability and gives some clue regarding the geophysical process involved in the observed area [8]. When working with high rate data, e.g., with a sampling frequency of 20 Hz for Jason- or Sentinel-3-series,

Manuscript received March 7, 2020; revised September 15, 2020 and February 12, 2021; accepted March 14, 2021. Date of publication May 5, 2021; date of current version December 23, 2021. *(Corresponding author: Corinne Mailhes.)*

Corinne Mailhes is with INPT, University of Toulouse, 31000 Toulouse, France, and also with TéSA, 31500 Toulouse, France (e-mail: corinne.mailhes@n7.fr).

Olivier Besson is with ISAE-SUPAERO, University of Toulouse, 31000 Toulouse, France, and also with TéSA, 31500 Toulouse, France (e-mail: olivier.besson@isae-supaero.fr).

Amandine Guillot and Sophie Le Gac are with the Centre National d'Etudes Spatiales (CNES), 31400 Toulouse, France (e-mail: amandine.guillot@cnes.fr; sophie.legac@cnes.fr).

Digital Object Identifier 10.1109/TGRS.2021.3071802

the white noise plateau appearing at short spatial scales corresponds to the assumed Gaussian instrumental noise [9].

Estimation of the slope α is done on the power spectral density (PSD) estimate in a log–log scale. To perform a reliable slope estimation, the PSD estimate has to have a variance sufficiently low. Therefore, the widely used spectral method is based on a cumulated (Welch) periodogram which consists of averaging a large number of periodograms of along-track SLA segments [8], [10]–[14]. This PSD averaging determines the spatial and temporal resolution of the resulting slope map, depending on the size of the area in latitude and longitude and on the time period from which the SLA signals are issued. If we take into account the resolutions currently targeted (10° (in latitude) by 10° (in longitude) and averaging over several months, or even several years of SLA data, the cumulated periodogram coupled with a least squares estimate is an effective and efficient method for estimating the slope.

However, it would be of interest to improve the spatial and temporal resolution of the slope estimates. Therefore, this article focuses on SLA slope estimation using a small number of signal samples, i.e., a single segment of a few thousand samples, corresponding to a single satellite pass in a very short time interval, over a given area, the number and the dates of samples used being directly related to the spatial and temporal resolution of the estimate.

The article is organized as follows. Section II recalls the methods widely used for spectral slope estimation to show their limitations when applied to short signal segments. Moreover, this section also describes the main interesting characteristics of SLA signals to highlight the difficulty of such a spectral estimation. Section III introduces the proposed spectral estimator referred to as autoregressive model combined with a warping of the frequency scale (ARWARP). To conduct a quantitative comparison between different methods, Section IV derives the Cramér–Rao bound (CRB) of the slope estimate. Furthermore, rather than performing linear regression on the spectral estimates, a new estimator of α is suggested, based on a model fitting of the spectral estimates. A statistical analysis of slope estimation using ARWARP is conducted on simulated SLA signals in Section V. An application to real data from the Sentinel-3 satellite is presented in Section VI. Conclusions and future works are finally reported in Section VII.

II. Problem Statement

Let us assume that N consecutive measurements of SLA are collected along the satellite track every $1/f_s$ seconds, f_s denoting the sampling frequency, and gathered in a vector $\boldsymbol{x} = [x(0)\ x(1) \ldots\ x(N-1)]^T$, the superscript ^{T} denoting the transpose operation. Assuming that $\boldsymbol{x}$ is a sample drawn from a wide-sense stationary process with PSD $S_x(f)$, our objective is to obtain an estimate $\hat{S}_x(f)$ of $S_x(f)$ from $\boldsymbol{x}$, that can take into account the frequency characteristics of SLA signals.

Since we are considering sampled data, through the article, f will denote the normalized frequency, i.e., the actual frequency (hertz) divided by f_s. Therefore, all figures of SLA spectra are plotted as a function of f. It is noted that if the sampling rate f_s in hertz corresponds to a ground spacing of d_s in kilometer, any normalized frequency f can be converted to the corresponding wavenumber f/d_s in cycles per kilometer (cpkm) or to the wavelength d_s/f in kilometer. To illustrate this, a double x-axis has been included in Figs. 1, 2, and 6.

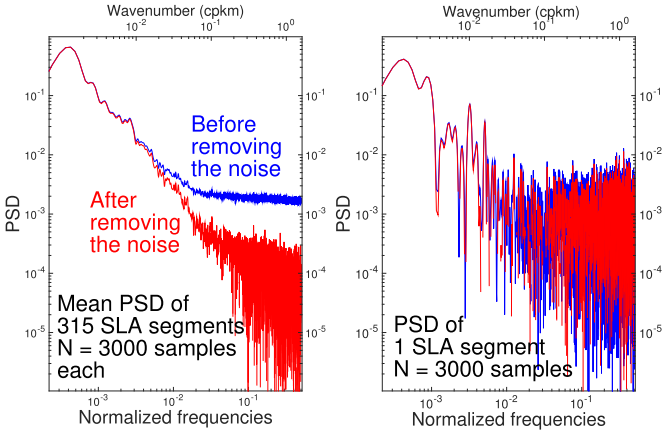

Fig. 1. Along-track Sentinel-3 altimeter wavenumber spectrum for the equator area within a box 20° × 20° centered at (0° N, 210° E): (Left) using a cumulated periodogram of 315 SLA segments of $N = 3000$ samples each, corresponding to seven months of data, and (Right) using a single periodogram on one SLA segment of $N = 3000$ samples (October–November 2016).

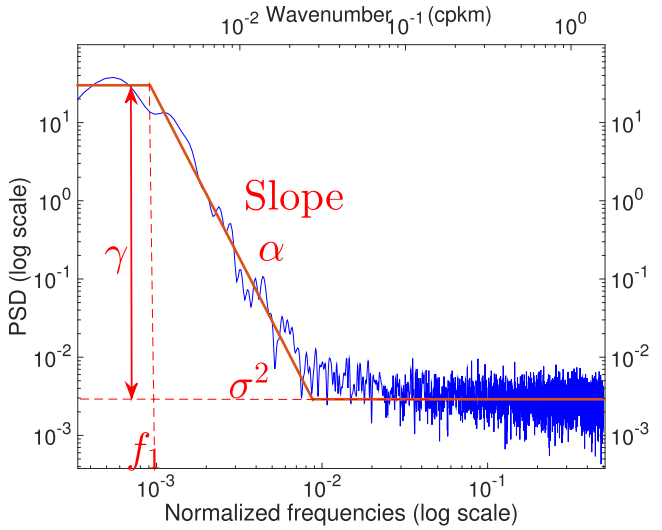

Fig. 2. Sentinel-3 SLA PSD (in blue) estimated by Welch periodogram ($L = 8$, $N = 3000$, 10% cosine taper window applied after detrending, zero-padding by a factor 3), compared with the expected shape in red.

A. Conventional Methods for SLA Spectral Slope Estimation

Estimation of the SLA spectral slope α is usually a two-step procedure [8], [10], [11], [13], [14]. First, an estimation of the PSD is done. Second, a least squares linear regression is applied on the log–log PSD representation within a specified frequency interval to estimate the slope α. To favor the performances of least squares linear regression, we need an estimated spectrum with a small variance. Therefore, PSD estimation is done on a large number of SLA samples, through

Fourier-based methods, classically a cumulated weighted periodogram (Welch periodogram) since averaging several PSD estimates is a way to reduce the variance of the estimation. This two-step procedure involves several parameters: the number of averaged PSD, the spatial box in latitude and longitude from which the corresponding SLA segments are selected, the weighting window, and the wavelength range for the linear fit. In [10], along-track altimeter data from TOPEIX/*Poseidon*, *Jason-1, ENVISAT* ,and *Geosat Follow-On* are selected within 10° (in latitude) by 20° (in longitude). Then, the wavenumber spectrum is calculated by averaging different PSDs over a four-year period which means using around 2000 SLA segments. The slope is calculated by a least squares regression for wavelengths between 100 and 300 km. In [11], the along-track observations whose PSD are averaged are covering seven years, the corresponding spatial boxes are $10° \times 10°$ and the linear fit is done between 70 and 250 km. However, the authors confirm that the presented results are not sensitive to the choice of the selected wavenumber band. The same procedure is applied in [13], specifying that the weighting window used in the cumulative periodogram is a 10% cosine taper. To improve the estimation performance and to robustify the results toward the choice of the frequency interval, [12] suggests to subtract the estimated noise level from the PSD estimation before performing the linear regression. This methodology is applied in [8] for *Jason-2, Cryosat-2* and SARAL/*Altika* along-track analysis, over seven months of data, within spatial boxes $10° \times 10°$ and with a linear fit over the range 95–280 km for slope estimation. In [15], the weighting window is a Hamming one and the number of spectral estimates which are averaged for each spatial box is of the order of 14 700.

These slope estimations result in a global map of the oceans whose spatial and temporal resolution depends on the size of the spatial box and on the time period of the selected SLA segments.

B. Improving the Temporal and Spatial Resolution

To improve the temporal and/or spatial resolution of the SLA slope estimates, one has to be able to perform this slope estimation on a SLA segment, either corresponding to a more restricted spatial box, either to a shorter time period, or both. Therefore, we are interested in estimating the SLA slope using a small number of samples, for example, a single segment of a few thousand of samples corresponding to a single satellite pass in a very short time interval. Fig. 1 on the left presents the result of the spectral analysis using classical Fourier-based methods as detailed in Section II-A, when cumulating 315 PSD estimations, with and without noise suppression as suggested by Xu and Fu [12]. One can obviously "see" the spectral slope, increased by removing the noise level (in red) which will make the slope estimate more robust. There is no doubt that when using a large number of SLA samples from long data records, Fourier-based methods are an efficient and effective mean to estimate the spectral slope. However, when looking for a higher temporal and/or spatial resolution and applying this methodology to a single segment of $N = 3000$ samples as on the right of Fig. 1, the variance of the PSD estimate is so high that removing the noise level does not bring any improvement and one can understand that slope estimation will be a difficult task. In this context, there is a need for another spectral estimator, not relying on a Fourier-based one, to analyze short segments of SLA signals with better bias and variance properties.

C. PSD Model of SLA

Before addressing estimation of SLA signal PSD, we would like to highlight some specific features of this PSD, since any appropriate PSD estimation method should take them into account.

The first issue concerns the shape of the PSD. As awaited from the quasigeostrophic theory [10], [16], the PSD of SLA signals exhibits a decrease of the type $f^{-\alpha}$, starting from some minimal frequency f_1. In other words, one can observe a line in a log–log representation. In addition to the signal component, thermal noise, which is usually modeled as a white Gaussian process, is present. Therefore, in a first approximation, a simplified model of SLA PSD is given by

$$S_x(f) = \sigma^2 + S_\alpha(f) \ = \sigma^2 + \begin{cases} C f_1^{-\alpha} & 0 \le f < f_1 \\ C f^{-\alpha} & f \ge f_1 \end{cases} \quad (1)$$

where σ^2 stands for the white noise power, and where the power at very low frequencies $C f_1^{-\alpha}$ is fixed by continuity arguments and from the fact that the PSD for $f < f_1$ is not known, or at least not easy to characterize as f_1 is very low. Indeed, this value of f_1 is usually chosen equal to a few bins of the SLA signal Fourier transform (FT), i.e., to k/N in normalized frequencies with $k = 3$ for example. It can be associated with the so-called energy-containing scale where the spectrum is leveling off [11]. The real data used in this article are from Sentinel-3 satellite, sampled at $f_s = 20$ Hz, which corresponds to a distance of 319 m between samples along the satellite track. Analyzing segments of $N = 3000$ samples of SLA signals leads to set $f_1 = 0.001$, as shown in Fig. 2, which is a very low normalized frequency corresponding to a spatial scale of around 320 km. This illustrates why precise characterization of the PSD for frequencies below f_1 is really questionable. Hence, the proposed model accounts for a constant value at frequencies below f_1. A second and important characteristic of the PSD of the signal component is that it lies in a very narrowband located at very low frequencies. Again, for the real data of Sentinel-3 used in this article, as can be seen in Fig. 2, the informative part of the slope area lies approximately in the interval $[0.001, 0.01]$ (equivalent to 320–30 km) which is a very small part of the total normalized frequency interval $[0, 0.5[$, located at very low frequencies. This is rather unusual in PSD estimation and calls for specific processing.

III. Proposed Spectral Estimator

A. Parametric Spectral Analysis

Parametric spectral analysis is an effective alternative to nonparametric Fourier-based analysis [17], [18]. It relies on a PSD model depending on a parameter vector $\boldsymbol{\theta}$ so that the PSD

estimation $S_x(f;\boldsymbol{\theta})$ amounts to that of $\boldsymbol{\theta}$, yielding an estimate $S_x(f;\hat{\boldsymbol{\theta}})$ where $\hat{\boldsymbol{\theta}}$ is an estimate of $\boldsymbol{\theta}$. Two main benefits have been advocated to support this parametric approach. First, with possibly a small number of parameters describing the PSD, accurate estimation can be conducted with a low number of samples. For SLA signals, this would allow us to estimate the slope on a small ocean area, with a few SLA samples (in the case of Sentinel-3, the distance between two consecutive samples is 319 m along the satellite track). Another advantage is that estimates of the form $S_x(f;\hat{\boldsymbol{\theta}})$ exhibit less variance than Fourier-based estimates, leading to smoother PSD, which will facilitate a reliable slope estimation in the case of SLA signals.

A very popular and understood PSD parametric model is the autoregressive (AR) one, due to the fact that obtaining the AR parameters reduces to solving a linear least-squares problem, for which computationally efficient algorithms have been proposed [17], [18]. Moreover, an AR model is of interest for a large class of signals since it consists in modeling a signal $x(n)$ as a linear combination of its past samples with an additive component representing the unexpected part of the signal

$$x(n) = -\sum_{\ell=1}^{p} a_\ell x(n-\ell) + e(n) \tag{2}$$

where p is the AR model order, a_ℓ is the ℓth AR coefficient, and $e(n)$ is the model error [namely the linear prediction error (LPE)]. The fitting of such a model to a signal leads to the following spectral estimator of $x(n)$:

$$S_{\mathrm{AR}}\left(f;\left[a_1\ \ldots\ a_p\ \sigma_e^2\right]\right) = \frac{\sigma_e^2}{\left|1+\sum_{\ell=1}^{p} a_\ell e^{-i2\pi\ell f}\right|^2} \tag{3}$$

where σ_e^2 is the LPE power. In the case of SLA signals, our experience is that AR modeling can work fine, provided that a sufficient AR model order (large number of parameters) is used. However, this is not fully satisfactory since we loose the interest of a model with few parameters and we do not take into account the problem specificities, namely that the spectral part of interest lies in very low frequencies while the rest of the frequency band contains mostly white noise.

B. Proposed Preprocessing: Warping

To account for the frequency distribution of the signal power, we use the basic idea of a nonuniform spectral representation, with a view to emphasize the lower part of the spectrum compared to the high-frequency part. This idea of using an unequal resolution related to the frequency is an old one, which goes back to the seventies [19], [20]. It has been extensively used for audio applications [21] where it is sometimes referred to as "frequency warping." The basic idea is to obtain a transformed sequence $y(n)$, which corresponds to an expansion over a set of orthogonal sequences $\psi_k(n)$, that is

$$x(n) = \sum_{k=-\infty}^{+\infty} y(k)\psi_k(n) \tag{4}$$

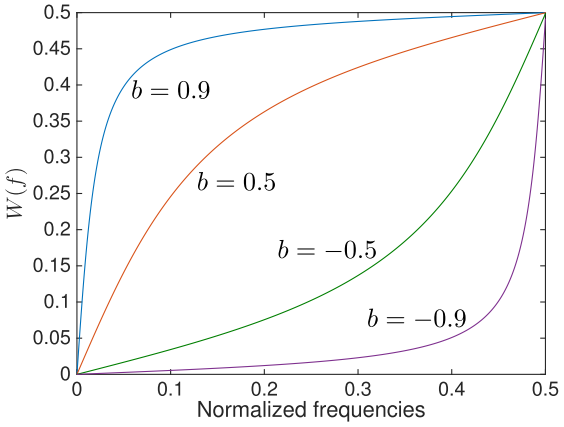

Fig. 3. Frequency warping function $W(f)$ for different values of b.

where the functions $\psi_k(.)$ should be chosen so that the FTs of $x(n)$ and $y(n)$ are related to one another by a function $W(f)$ such that

$$Y(W(f)) = X(f) \text{ i.e.,}$$
$$\sum_{k=-\infty}^{+\infty} y(k)e^{-j2\pi kW(f)} = \sum_{n=-\infty}^{+\infty} x(n)e^{-j2\pi nf}. \tag{5}$$

Hence, a conventional FT of $y(n)$ over equally spaced frequencies yields a nonequally spaced frequency analysis for $x(n)$. A significant advantage of this technique is that it can be implemented very easily from digital filters. Various choices exist for the sequences $\psi_k(n)$ which result in different nonlinear functions $W(f)$. Since they exhibit good properties and are widely used in warping methods, this article uses Laguerre functions [22], leading to

$$W(f) = f + \frac{1}{\pi}\arctan\left(\frac{b\sin(2\pi f)}{1-b\cos(2\pi f)}\right) \tag{6}$$

where the parameter $b \in [-1, 1]$ impacts the shape of the function $W(f)$, as can be seen in Fig. 3. In our application, one wishes to dilate low frequencies while compressing high frequencies, leading to the constraint $b > 0$.

C. Proposed Spectral Analysis: ARWARP

For SLA signal analysis, we propose to use frequency warping as a preprocessing step, which enhances the low-frequency components before an AR spectral analysis. A linear regression is finally conducted on the resulting AR estimator allowing the slope α to be estimated, as illustrated in Fig. 4. The warping preprocessing might be combined with any spectral analysis method. However, based on the benefits of parametric methods detailed above, AR modeling has been preferred for SLA analysis. The pair (frequency warping, AR modeling) will be referred to as ARWARP in the sequel.

ARWARP requires the tuning of three parameters: the warping coefficient b, the number of warped samples M, and the AR model order p. The selected values of b and M usually result from some tradeoff. More precisely, the warping coefficient b is directly linked to a so-called turning point

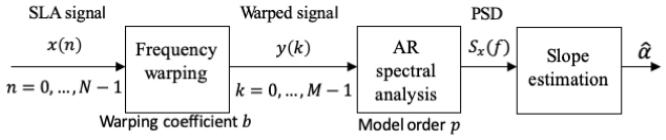

Fig. 4. Proposed SLA processing combining warping, AR modeling (ARWARP), and slope estimation.

frequency f_w [21]

$$b = \cos(2\pi f_w). \tag{7}$$

For $b > 0$, the PSD is sampled with higher resolution at frequencies lower than f_w, and lower resolution at frequencies higher than f_w. For SLA signals, f_w should correspond to the end of the slope region in a log–log scale (also corresponding to the beginning of the noise floor), i.e., $f_w \simeq 0.01$ in normalized frequencies, as observed in Fig. 2, which corresponds to $b = 0.99$.

The input SLA signal being of finite length (N samples), the warped sequence should be of infinite size [19]. However, from a practical point of view, only M samples of the warped sequence are computed. The influence of the warping sequence truncation has been studied in [22]: taking into account the total group propagation time of the Laguerre warping system, the minimum number of warped samples allowing a quasi-reversible transformation is defined by

$$M = N\frac{1+|b|}{1-|b|}. \tag{8}$$

It is noted that for $N = 3000$ and $b = 0.99$, we obtain $M = 597\,000$ which induces a high computational cost in the warping step. To reduce the value of M, we have chosen $b = 0.9$, corresponding to a value of M more than ten times lower, i.e., $M = 57\,000$ and a turning point frequency of $f_w = 0.07$, which is acceptable in view of Fig. 2.

Finally, the model order p needs to be adjusted. One might think of using classical AR model order criteria such as Akaike or minimum description length (MDL) [17], [18], [23]. However, these criteria are more adapted to line spectra, which is not the case for SLA signals. The model order p has to be low enough to guarantee a "smooth" spectral behavior. A reasonable choice is $p \in \{5, \ldots, 9\}$.

Once the ARWARP parameters have been set, one can compute the ARWARP spectral estimator as follows:

$$S_{\mathrm{AW}}(f) = \frac{\sigma_e^2}{\left|1+\sum_{\ell=1}^{p} a_\ell e^{-i2\pi\ell W(f)}\right|^2}|\Lambda_0(f)|^2 \tag{9}$$

where $a_\ell, \ell = 1, \ldots, p$ are the AR coefficients estimated using any linear prediction algorithm applied to the warped sequence $y(k), k = 0, \ldots, M-1$, σ_e^2 is the LPE power and $\Lambda_0(f)$ is the lowpass filter (in the case of $b > 0$) corresponding to the zero-order Laguerre sequence [22].

Once the PSD (9) has been computed, the slope α has to be estimated. The problem of slope estimation performed on a log–log spectral representation is the focus of Section IV. The full estimation strategy is summarized in Fig. 4.

IV. Bounds and Estimation of the Slope α

While Section III-B and III-C focused on estimating $S_x(f)$, let us now study the problem of the slope estimation in the model (1). First, we derive the CRBs to the variance of the estimates of the different model parameters, including the slope α. Second, two different estimation methods are proposed that rely on the ARWARP or Fourier-based PSD estimates.

A. Cramér–Rao Bound

The CRB for estimation of a vector parameter $\boldsymbol{\theta}$ from observation of $\boldsymbol{x} = [x(0) \ \ldots \ x(N-1)]^T$ provides the lowest variance that any unbiased estimator can achieve [24]. Therefore, whatever the problem, it constitutes a reference to which any estimator can be compared, especially when no estimator is known to achieve the bound, which is the most usual situation. Additionally, the CRB provides a quantitative measure of how difficult is the estimation problem and, as such, it bears much interest for SLA signals.

The $\mathrm{CRB}(\boldsymbol{\theta})$ is obtained as the inverse of the Fisher information matrix (FIM) $\boldsymbol{F}(\boldsymbol{\theta})$, which depends on the second-order derivatives of the log-likelihood function (LLF). For zero-mean Gaussian distributed signals, the LLF depends only on the signal correlation, which means that derivation of the CRB requires an explicit expression of the signal correlation as a function of $\boldsymbol{\theta}$. Unfortunately for SLA signals which are characterized in the spectral domain, as in (1), this is not the case as the inverse FT of (1) cannot be obtained analytically as a function of $\boldsymbol{\theta}$. Therefore, it would be more suitable to have an expression of the FIM which would depend on $\boldsymbol{\theta}$ through $S_x(f;\boldsymbol{\theta})$. Such an expression was found by Kay [24] and Whittle [25] who shows that for a Gaussian process the *asymptotic FIM* is given by

$$\begin{aligned}[\boldsymbol{F}_{\mathrm{as}}(\boldsymbol{\theta})]_{k,\ell} &= \frac{N}{2}\int_{-1/2}^{1/2}\frac{\partial \log S_x(f;\boldsymbol{\theta})}{\partial\theta_k}\frac{\partial \log S_x(f;\boldsymbol{\theta})}{\partial\theta_\ell}df \\ &= \frac{N}{2}\int_{-1/2}^{1/2}\frac{1}{S_x^2(f;\boldsymbol{\theta})}\frac{\partial S_x(f;\boldsymbol{\theta})}{\partial\theta_k}\frac{\partial S_x(f;\boldsymbol{\theta})}{\partial\theta_\ell}df. \end{aligned}\tag{10}$$

While this expression holds only for large N, it has been shown to come rather close to the exact CRB even in short data samples, say $N = 100$, see e.g., [26]. Therefore, not only (10) is well-suited for SLA signals, but it is also meaningful since no efficient estimator exits for finite N (only asymptotic efficiency is possible) and one can conjecture that the exact CRB will be rather close to the asymptotic CRB with the number of samples we consider, namely $N = 3000$.

To obtain the CRB, let us rewrite (1) as

$$S_x(f;\boldsymbol{\theta}) = \begin{cases} \sigma^2(1+\gamma) & f < f_1 \\ \sigma^2\left(1+\gamma f^{-\alpha} f_1^{\alpha}\right) & f \geq f_1 \end{cases} \tag{11}$$

and let us define $\boldsymbol{\theta} = [\gamma \ \alpha \ \sigma^2]^T$. Differentiating (11) yields

$$\frac{\partial \log S_x(f;\boldsymbol{\theta})}{\partial\gamma} = \begin{cases} (1+\gamma)^{-1} & f < f_1 \\ \dfrac{f_1^{\alpha}}{f^{\alpha}+\gamma f_1^{\alpha}} & f \geq f_1 \end{cases} \tag{12a}$$

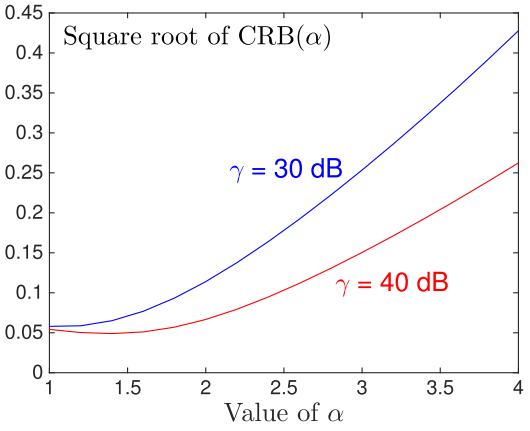

Fig. 5. Square root of CRB(α) for the model (11) versus α ($\gamma = 30$ dB in blue and 40 dB in red, $f_1 \leftrightarrow 319$ km and $N = 3000$).

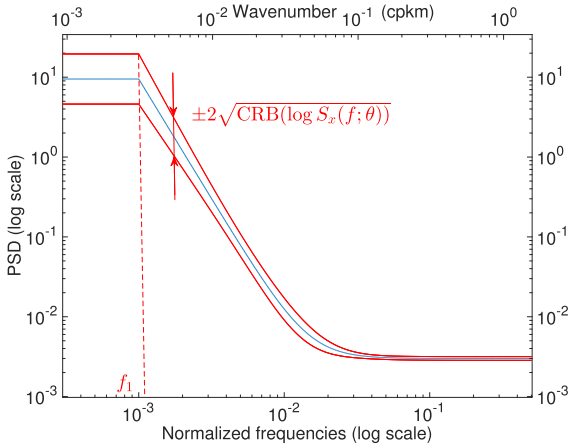

Fig. 6. DSP model (11) in blue and the interval at $\pm 2\sqrt{\text{CRB}(\log S_x(f;\boldsymbol{\theta}))}$ in red, with $\gamma = 35$ dB, $\sigma^2 = 0.003$, $\alpha = 3$ and $N = 3000$.

$$\frac{\partial \log S_x(f;\boldsymbol{\theta})}{\partial \alpha} = \begin{cases} 0 & f < f_1 \\ \dfrac{\gamma f_1^{\alpha}}{f^{\alpha} + \gamma f_1^{\alpha}} \log\left(\dfrac{f_1}{f}\right) & f \geq f_1 \end{cases} \tag{12b}$$

$$\frac{\partial \log S_x(f;\boldsymbol{\theta})}{\partial \sigma^2} = \sigma^{-2} \tag{12c}$$

which provides all necessary entries to compute the asymptotic FIM. While analytical evaluation of the integrals in (10) cannot be given, a numerical integration is possible, which provides the elements of the asymptotic FIM. Inversion of the latter provides the asymptotic CRB for estimation of $\boldsymbol{\theta}$. Bearing in mind that the exact CRB is not achievable, any estimator whose variance is "close" to the asymptotic CRB can be deemed to be a good estimator.

The expressions in (12) call for some comments:

1) The CRB for σ^2 given by $[\boldsymbol{F}_{\text{as}}(\boldsymbol{\theta})]^{-1}_{3,3}$ is proportional to (σ^4/N), the proportionality term depending on the other parameters f_1, γ, α which is a usual behavior,
2) The CRBs for γ and α given by $[\boldsymbol{F}_{\text{as}}(\boldsymbol{\theta})]^{-1}_{1,1}$ and $[\boldsymbol{F}_{\text{as}}(\boldsymbol{\theta})]^{-1}_{2,2}$ do not depend on σ^2, they only depend on f_1, γ, α and are proportional to $(1/N)$.

For illustration purposes, Fig. 5 displays the asymptotic CRB(α) versus α for values of γ observed on real SLA signals from Sentinel-3 and $f_1 = 0.001$ (corresponding to 319 km).

This shows that when α increases, it is more and more difficult to estimate it, which is an expected behavior. It should also be noted that, as γ increases, the CRB decreases which is logical since the gap between the power at lower frequency and the power at high frequency increases. To give more precise results, Fig. 5 shows that a precision of less than 10% with $\gamma = 40$ dB is impossible to achieve when estimating α around 3, while for $\gamma = 30$ dB, the precision cannot be below 16%, for α of the same order, considering an uncertainty interval of $\pm 2(\text{CRB}(\alpha))^{1/2}$ and keeping in mind that this is an optimistic and asymptotic bound.

The previous theory also allows us to derive a bound for estimation of $\log S_x(f;\boldsymbol{\theta})$ as

$$\text{CRB}(\log S_x(f;\boldsymbol{\theta})) = \frac{\partial \log S_x(f;\boldsymbol{\theta})}{\partial \boldsymbol{\theta}^T} \text{CRB}(\boldsymbol{\theta}) \frac{\partial \log S_x(f;\boldsymbol{\theta})}{\partial \boldsymbol{\theta}} \tag{13}$$

where the derivatives are given by (12). In Fig. 6, we display the PSD model (11) and the interval at $\pm 2(\text{CRB}(\log S_x(f;\boldsymbol{\theta})))^{1/2}$. This highlights that the lower the frequency, the more difficult it is to have a precise estimation of the PSD, which is an awaited behavior.

B. Estimation of α

We now address the issue of proposing an estimator of α, using a two-step approach. First, an estimate $\hat{S}_x(f)$ is obtained, using for example one of the two methods proposed earlier, i.e., the periodogram or the ARWARP estimator. Second, we perform a fitting between $\log \hat{S}_x(f)$ and $\log S_x(f;\boldsymbol{\theta})$, i.e., $\boldsymbol{\theta}$ is estimated by solving

$$\min_{\boldsymbol{\theta}} \int_{f_{\min}}^{f_{\max}} [\log \hat{S}_x(f) - \log S_x(f;\boldsymbol{\theta})]^2 df. \tag{14}$$

$S_x(f;\boldsymbol{\theta})$ being the SLA model (11). In practice, the integral is replaced by a summation over a grid of frequencies spanning the interval $[f_{\min}, f_{\max}]$. Alternatively, to have a simpler method, one can investigate a simple linear regression over $\log \hat{S}_x(f)$ and estimate the slope by solving

$$\min_{\alpha,\beta} \int_{f^-}^{f^+} [\log \hat{S}_x(f) - \alpha f - \beta]^2. \tag{15}$$

Again, integrals are replaced by finite sums and a simple linear least-squares problem needs to be solved. This last method is the one used in most publications [8], [10], [11], [13], [14].

V. Validation on Simulated Signals

To validate our proposed approach, one has to compare with the conventional method used for SLA slope estimation, i.e., based on a periodogram which, in this case of short SLA segments, cannot be an averaged one but only a single periodogram including a weighting window $w(n)$

$$I_w(f) = \frac{1}{N} \left| \sum_{n=0}^{N-1} w(n) x(n) e^{-i2\pi nf} \right|^2. \tag{16}$$

Then, four different estimators of the SLA slope α can be compared. They are designed by three letters in what follows and described hereafter:

LRP: Linear regression (15) over a log-periodogram (16).

MFP: Model fitting (14) over a log-periodogram (16).

LRA: Linear regression (15) over an ARWARP (9).

MFA: Model fitting (14) over an ARWARP (9).

The four estimators LRP, MFP, LRA, and MFA are compared in terms of mean-square error (MSE) to the asymptotic CRB. Section V-A presents the simulation model used to generate SLA signals with a given slope. The results of Monte-Carlo simulations are analyzed in Section V-B.

A. Simulation Model

Simulated SLA signals were generated as Gaussian vectors through a Cholesky decomposition of the correlation matrix. The latter is computed from the inverse FT of $S_\alpha(f)$ in (1), with the addition of the noise power σ^2 in the diagonal terms

$$\boldsymbol{x} \sim \mathcal{N}(\boldsymbol{0}, \boldsymbol{R}_{xx})$$

with

$$\boldsymbol{R}_{xx} = \begin{pmatrix} r_0 + \sigma^2 & r_1 & \cdots & r_{N-1} \\ r_1 & r_0 + \sigma^2 & \cdots & r_{N-2} \\ \vdots & \vdots & \ddots & \vdots \\ r_{N-1} & r_{N-2} & \cdots & r_0 + \sigma^2 \end{pmatrix}$$

and

$$\{r_0, \ldots, r_{N-1}\} = \mathrm{FT}^{-1}[S_\alpha(f)]. \tag{17}$$

The Gaussian assumption has been validated on real data. The corresponding MATLAB code for the generation of SLA signals is available in [27].

Monte Carlo simulations of SLA signals with a known slope value allow to evaluate the statistics of the four estimates LRP, MFP, LRA, and MFA. We also compare these estimations to the CRB which provides a reference.

This approach is illustrated in Fig. 7 where $N = 3000$ samples of a signal whose PSD is given by (11) were generated. Both a weighted periodogram (16) and an ARWARP spectral estimate (9) were computed. These estimates were used in (14) and (15) to obtain estimates of α, represented by either a red segment corresponding to the linear regression result, or a red fitted spectral model when using (14), all compared to the black dotted line which is the "ground truth." As can be observed, ARWARP spectral estimate exhibits less variance than the periodogram, which was expected. The following numerical simulations provide quantitative analysis of the performance of these methods.

B. Statistical Analysis

Based on the above simulation model, 1000 Monte-Carlo simulations were run for a SLA signal of $N = 3000$ samples with PSD (1), the frequency f_1 corresponding to a distance $d_1 = 319$ km (i.e., a normalized frequency $f_1 = 10^{-3}$) and a white noise level fixed to $\sigma^2 = 0.003$ (to be coherent with Sentinel-3 real data). Fourier-based spectrum estimation was

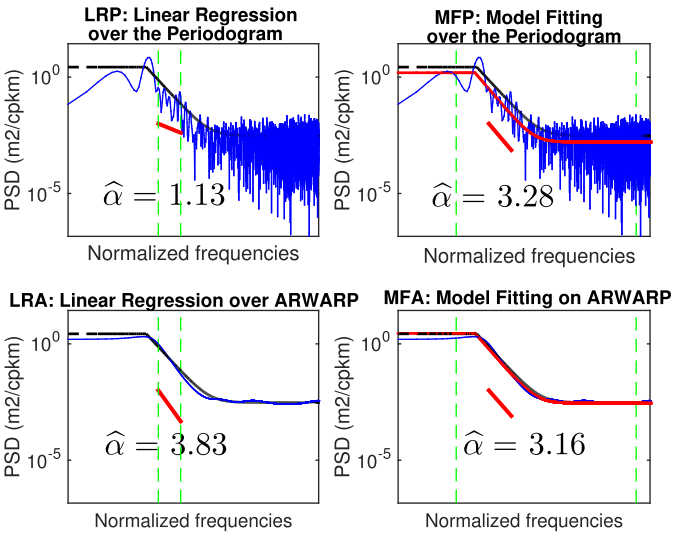

Fig. 7. Slope estimates (Left) by linear regression and (Right) by model fitting between the two vertical dashed green lines over (Top) a periodogram (10% cosine taper window applied after detrending, zero-padding by a factor 3) and (Bottom) an ARWARP ($p = 7$, $b = 0.9$, $M = 57\,000$), of a simulated SLA signal ($N = 3000$, $\alpha = 3$, $\gamma = 30$ dB).

TABLE I

CRB AND MSE OF SLOPE ESTIMATES USING THE FOUR PROPOSED ESTIMATORS WITH $N = 3000$ SAMPLES OF SLA SIGNAL

α	2	2.5	3	3.5	4
CRB	0.054	0.063	0.068	0.071	0.072
MSE of LRP	0.763	0.751	0.677	0.570	0.537
MSE of MFP	0.286	0.214	0.153	0.126	0.134
MSE of LRA $p = 5$	0.197	0.231	0.159	0.125	0.232
MSE of MFA $p = 5$	0.080	0.124	0.164	0.274	0.681
MSE of LRA $p = 7$	0.230	0.208	0.128	0.098	0.275
MSE of MFA $p = 7$	0.085	0.104	0.141	0.265	0.693

conducted using a periodogram with a 10% cosine taper window applied after detrending and zero-padding by a factor 3. For the ARWARP model, the warping parameter was $b = 0.9$ and different values of the model order were considered, i.e., $p \in \{5, 7, 9\}$.

Linear regression is performed following (15) between f^- and f^+ corresponding to 45 and 160 km, while model fitting is done, following (14) with $f_{\min}$ and $f_{\max}$ corresponding to 1 and 630 km (dashed green vertical lines in Fig. 7).

Fig. 8 displays the boxplots of the bias between the estimated and theoretical values of α versus different values of α, while the corresponding values of the MSE are reported in Table I.

From inspection of them, the following conclusions can be drawn regarding slope estimation:

1) When spectral estimation is done through Fourier analysis, Table I shows that slope estimation using linear regression gives a MSE around 10 times the CRB which means that there is space for improvement.
2) When spectral estimation is done through Fourier analysis, model fitting should be preferred: the MSEs are lower than when performing linear regression, whatever the slope value. This is highlighted on the two left

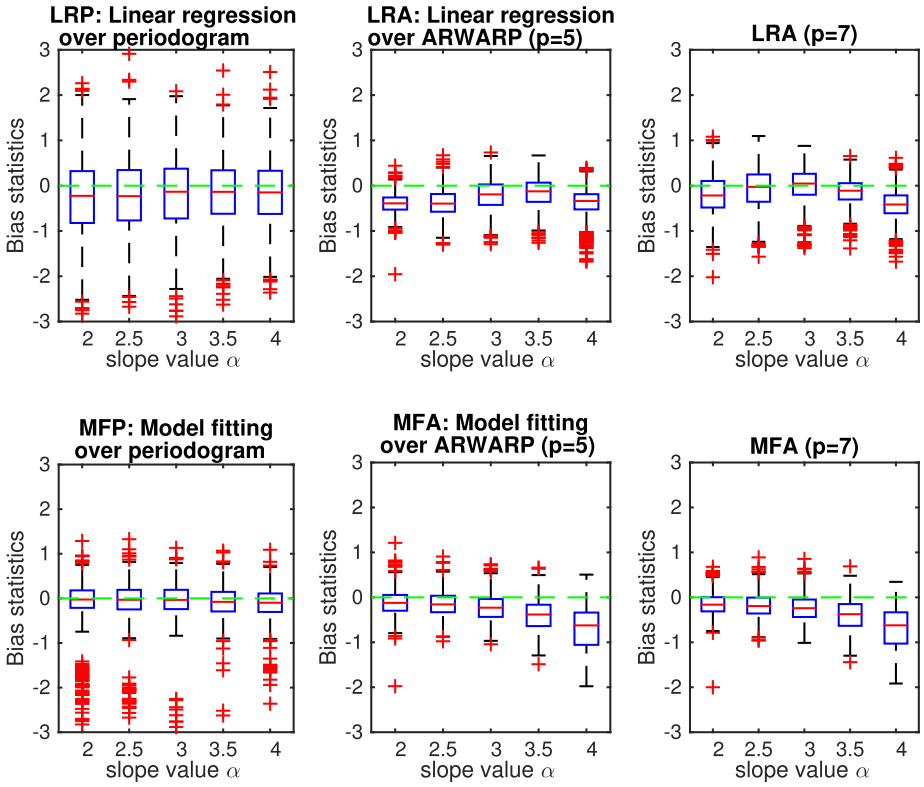

Fig. 8. Statistics (boxplots) of slope bias on 1000 sequences of simulated SLA ($N = 3000$): (Left) estimation using periodogram, (Middle) ARWARP of orders 5, and (Right) 7, (Top) with linear regression and (Bottom) model fitting. In each box plot, the central mark is the median, the edges of the box are the 25th and 75th percentiles, the whiskers extend to the most extreme datapoints the algorithm considers to be not outliers, and the outliers are plotted individually in red.

figures of Fig. 8: the variance of estimation is smaller with model fitting.

3) However, model fitting on Fourier spectrum sometimes fails, leading to spurious results (red marks in Fig. 8), while model fitting on ARWARP spectrum seems to be more robust (less outliers).
4) When spectral estimation is done through ARWARP, model fitting does not bring a systematic improvement, compared to linear regression (see Table I): this may be explained by the fact that the ARWARP spectral estimation is smooth and linear regression performs well. For small values of slope, model fitting leads to lower MSEs, while for high slope values, linear regression should be preferred.
5) When spectral estimation is done through ARWARP, increasing the model order does not bring much improvement: the behavior of the method remains the same: with model fitting, the bias and the variance of the estimation increase with the value of the slope, while linear regression leads to almost the same results for model order of five and seven (simulations have shown that increasing more the model order increases the MSE).

Finally, based on these results on simulated SLA signals, two estimates are of interest for slope estimation: linear regression on ARWARP (LRA $p = 5$) and model fitting on the periodogram (MFP). Both have the same performance in terms of MSE, whatever the slope value, being around three times the CRB. Remembering that the latter is very optimistic, one can state that the proposed estimators are rather accurate. The main interest of model fitting on the periodogram is the low computational cost but it can bring unacceptable bias, with estimated values going from -1 to 0.5 for a simulated SLA slope of 2 for example (see outliers of the bottom left boxplots of Fig. 8). Therefore, linear regression on ARWARP (LRA) should be preferred, although the computational cost may be higher.

The interest of linear regression on ARWARP compared to the three other estimators has been shown on simulated SLA signals. Section VI presents the application of these estimators on real SLA signals.

VI. Validation on Real Signals

A. SLA Around the Equator

First, we apply the proposed ARWARP method on Sentinel-3 real data measured around the Equator in an area where the slope is known to have low values and to be mostly stationary. Fig. 9 presents the result of slope estimation on 52 segments of $N = 3000$ samples issued from cycle 11 of Sentinel-3A sampled at 20 Hz, within a box $20° \times 20°$ centered at (0°S, 150°W), between November and December 2016: on the left with linear regression over the periodogram in blue (LRP) and ARWARP in red (LRA) and on the right with model fitting over the periodogram in blue (MFP) and ARWARP in red (MFA). Since quite constant values of the slope are expected,

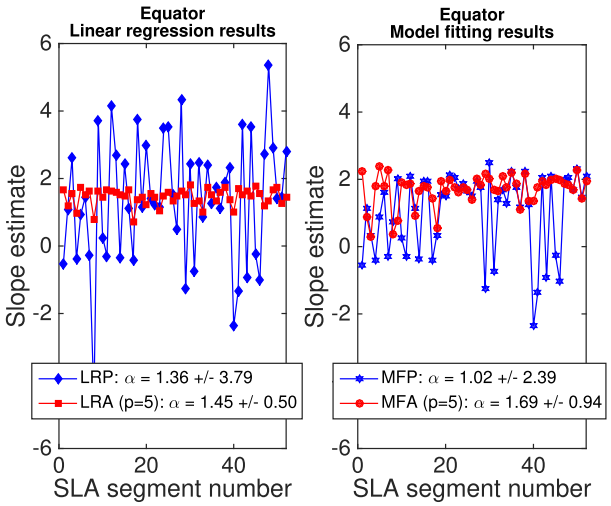

Fig. 9. Slope estimates on SLA segments of the Equator area, sampled at 20 Hz, within a box 20° × 20° centered at (0°S, 150°W), between November and December 2016 ($N = 3000$), using periodogram (blue), ARWARP ($p = 5$, red). The mean value of the estimated slopes is also reported with an error interval of ± twice the standard deviation. (Left) Using linear regression between 90 and 200 km. (Right) Using model fitting on the whole spectrum.

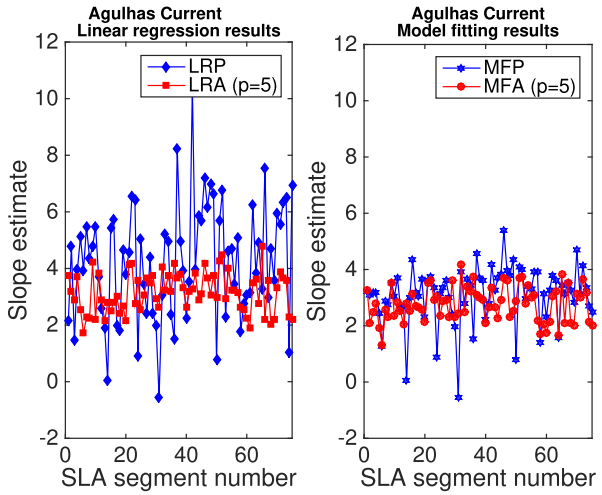

Fig. 10. Slope estimation on SLA segments of the Agulhas current area, sampled at 20 Hz, within a box 20° × 13° centered at (35°S, 26.5°E), between October 2016 and May 2017 ($N = 3000$), using periodogram (blue) and ARWARP (order $p = 5$, red). (Left) Using linear regression between 90 and 200 km. (Right) Using model fitting on the whole spectrum.

the mean value with a confidence interval at twice the standard deviation is given for each estimator in the legend.

As can be seen, slope estimation via periodogram (blue curves) gives spurious results with an unacceptable variance along the different segments. This shows clearly that a Fourier-based spectral estimate cannot be used for slope estimation on short SLA segments [14], which explains why averaging several periodograms is necessary. However, on the same short SLA segments, ARWARP estimates yield quite constant values of the slope, as expected in this Equator area. Especially, the linear regression over the ARWARP model (LRA, red curve on the left) gives values of the slope around $\alpha = 1.45$ and a small variance, as expected from a physical point of view. It is noted that a classical Welch (cumulated) periodogram on these 52 segments gives an estimation of the slope $\widehat{\alpha} = 1.51$, which make the LRA results reliable.

B. SLA in the Agulhas Current

Let us now consider SLA segments from the Agulhas Current, which is a region with high eddy kinetic energy and where higher and different slope values are expected. Fig. 10 displays slope estimates obtained on 75 different SLA segments ($N = 3000$), issued from cycles 10 to 17 of Sentinel-3A, sampled at 20 Hz, within a box 20° × 13° centered at (35°S, 26.5°E), between October 2016 and May 2017. In this case also, linear regression over the periodogram (LRP, blue curve on the left) obviously gives spurious and unreliable results. The same behavior is observed with model fitting on the periodogram (blue curve on the right) even if less irrelevant results are obtained. ARWARP estimates are more coherent and based on the previous validations on simulated SLA signals and on the homogenous Equator area, one can trust these results. In an area of the ocean where it will be difficult to average several periodograms without questioning about the stationarity of the different SLA segments, the ARWARP model allows PSD and slope estimations on each individual segment, i.e., corresponding to a small area on the ocean.

VII. Conclusion

In this article, we addressed the problem of PSD and slope estimation of short SLA segments, for example, to analyze regions of the ocean with high eddy kinetic energy. First, the asymptotic CRB of the estimation variance was derived. Even if this is only an asymptotic result for an unbiased estimator, this bound is a reference to which any estimator has to be compared. We showed that the usual estimator based on a linear regression over a weighted periodogram gives MSE values ten times higher than the CRB, which shows that there is space for improvement. Second, this article proposed a new method to estimate the slope of SLA signals based on a combination of frequency warping, AR modeling, and linear regression. This method showed improved results compared to Fourier-based strategies for simulated SLA signals. The resulting estimator can be considered as a good one, with a variance around three times the CRB. This improvement has also been observed on real Sentinel-3 data. The proposed ARWARP model makes PSD and slope estimations possible on a short SLA segment, i.e., allows spatial resolution of the estimates to be improved. Future works include validation on more real data, which is encouraged using the MATLAB code available in [27].

References

[1] P. Y. L. Traon and R. Morrow, "Ocean currents and eddies," in *Satellite Altimetry and Earth Sciences: A Handbook of Techniques and Applications*, L. Fu and A. Cazenave, Eds. New York, NY, USA: Academic, 2001, ch. 3, pp. 171–215.

[2] J. Lambin *et al.*, "The OSTM/Jason-2 mission," *Mar. Geodesy*, vol. 33, no. 1, pp. 4–25, Aug. 2010.

[3] C. Donlon *et al.*, "The sentinel-3 mission: Overview and status," in *Proc. IEEE Int. Geosci. Remote Sens. Symp.*, Jul. 2012, pp. 1711–1714.

[4] L. Aouf and J.-M. Lefèvre, "On the impact of the assimilation of SARAL/AltiKa wave data in the operational wave model MFWAM," *Mar. Geodesy*, vol. 38, no. 1, pp. 381–395, Sep. 2015.

[5] S. Calmant, F. Seyler, and J. F. Cretaux, "Monitoring continental surface waters by satellite altimetry," *Surveys Geophys.*, vol. 29, nos. 4–5, pp. 247–269, Oct. 2008.

[6] D. Wingham *et al.*, "CryoSat: A mission to determine the fluctuations in Earth's land and marine ice fieldss," *Adv. Space Res.*, vol. 37, no. 4, pp. 841–871, 2006.

[7] D. Stammer, "Global characteristics of ocean variability estimated from regional TOPEX/POSEIDON altimeter measurements," *J. Phys. Oceanogr.*, vol. 27, no. 8, pp. 1743–1769, Aug. 1997.

[8] C. Dufau, M. Orsztynowicz, G. Dibarboure, R. Morrow, and P. L. Traon, "Mesoscale resolution capability of altimetry: Present and future," *J. Geophys. Res., Oceans*, vol. 121, no. 7, pp. 4910–4927, Jul. 2016.

[9] G. Dibarboure *et al.*, "Investigating short-wavelength correlated errors on low-resolution mode altimetry," *J. Atmos. Ocean. Technol.*, vol. 31, no. 6, pp. 1337–1362, Jun. 2014.

[10] P. Y. Le Traon, P. Klein, B. L. Hua, and G. Dibarboure, "Do altimeter wavenumber spectra agree with the interior or surface quasigeostrophic theory?" *J. Phys. Oceanogr.*, vol. 38, no. 5, pp. 1137–1142, May 2008.

[11] Y. Xu and L.-L. Fu, "Global variability of the wavenumber spectrum of oceanic mesoscale turbulence," *J. Phys. Oceanogr.*, vol. 41, no. 4, pp. 802–809, Apr. 2011.

[12] Y. Xu and L.-L. Fu, "The effects of altimeter instrument noise on the estimation of the wavenumber spectrum of sea surface height," *J. Phys. Oceanogr.*, vol. 42, no. 12, pp. 2229–2233, Dec. 2012.

[13] J. G. Richman, B. K. Arbic, J. F. Shriver, E. J. Metzger, and A. J. Wallcraft, "Inferring dynamics from the wavenumber spectra of an eddying global ocean model with embedded tides," *J. Geophys. Res., Oceans*, vol. 117, no. C12, Dec. 2012, Art. no. C12012.

[14] S. Wang, F. Qiao, D. Dai, and X. Zhou, "Anisotropy of the sea surface height wavenumber spectrum from altimeter observations," *Sci. Rep.*, vol. 9, no. 1, pp. 1–10, 2019, doi: 10.1038/s41598-019-52328-w.

[15] S. Biri, N. Serra, M. G. Scharffenberg, and D. Stammer, "Atlantic sea surface height and velocity spectra inferred from satellite altimetry and a hierarchy of numerical simulations," *J. Geophys. Res., Oceans*, vol. 121, no. 6, pp. 4157–4177, Jun. 2016.

[16] X. Capet, P. Klein, B. L. Hua, G. Lapeyre, and J. C. Mcwilliams, "Surface kinetic energy transfer in surface quasi-geostrophic flows," *J. Fluid Mech.*, vol. 604, pp. 165–174, Jun. 2008.

[17] P. Stoica and R. L. Moses, *Spectral Analysis of Signals*. Upper Saddle River, NJ, USA: Pearson, 2005.

[18] S. M. Kay, *Modern Spectral Estimation: Theory and Applications*. Englewood Cliffs, NJ, USA: Prentice-Hall, 1988.

[19] A. Oppenheim, D. Johnson, and K. Steiglitz, "Computation of spectra with unequal resolution using the fast Fourier transform," *Proc. IEEE*, vol. 59, no. 2, pp. 299–301, Feb. 1971.

[20] A. V. Oppenheim and D. H. Johnson, "Discrete representation of signals," *Proc. IEEE*, vol. 60, no. 6, pp. 681–691, Jun. 1972.

[21] A. Härmä, M. Karjalainen, L. Savioja, V. Välimäki, U. K. Laine, and J. Huopaniemi, "Frequency-warped signal processing for audio applications," *J. Audio Eng. Soc.*, vol. 48, no. 11, pp. 1011–1031, Nov. 2000.

[22] G. Evangelista and S. Cavaliere, "Frequency-warped filter banks and wavelet transforms: A discrete-time approach via Laguerre expansion," *IEEE Trans. Signal Process.*, vol. 46, no. 10, pp. 2638–2650, Oct. 1998.

[23] P. Stoica and Y. Selen, "Model order selection: A review of information criterion rules," *IEEE Signal Process. Mag.*, vol. 21, no. 4, pp. 36–47, Jul. 2004.

[24] S. M. Kay, *Fundamentals of Statistical Signal Processing: Estimation Theory*. Englewood Cliffs, NJ, USA: Prentice-Hall, 1993.

[25] P. Whittle, "The analysis of multiple stationary time series," *J. Roy. Stat. Soc. B*, vol. 15, no. 1, pp. 125–139, 1953.

[26] B. Porat and B. Friedlander, "The exact cramer-rao bound for Gaussian autoregressive processes," *IEEE Trans. Aerosp. Electron. Syst.*, vol. AES-23, no. 4, pp. 537–542, Jul. 1987.

[27] C. Mailhes and O. Besson, *MATLAB Code for SLA Analysis*. Accessed: Feb. 2020. [Online]. Available: https://www.tesa.prd.fr/software-tesa.p56.html

Corinne Mailhes (Member, IEEE) received the Engineering degree in electronics and signal processing and the Ph.D. degree in signal processing from the University of Toulouse (ENSEEIHT), Toulouse, France, in 1986 and 1990, respectively.

She is a Full Professor with the University of Toulouse (ENSEEIHT) and a Member of the IRIT Laboratory (UMR 5505 of the CNRS), Toulouse. Since November 2013, she has been the Head of TeSA Laboratory, Toulouse. Her research interests are centered on statistical signal processing, with particular interests in spectral analysis and altimetry.

Olivier Besson received the Ph.D. degree in signal processing from the Institut National Polytechnique Toulouse, Toulouse, France, in 1992.

From 1993 to 2007, he was a Professor of signal processing with the Department of Avionics and Systems, ENSICA, Toulouse. Since 2007, he has been with ISAE-SUPAERO, Toulouse, where he is the Head of the Ph.D. Program Office. His research interests include adaptive array processing, detection, estimation, and multivariate analysis with applications in radar processing and hyperspectral imaging.

Amandine Guillot received the Engineering degree in aerospace and signal processing from the Ecole Nationale Supérieure de Construction Aéronautique (ISAE Supaéro), Toulouse, France, in 2005.

In 2007, she joined the Center National d'Etudes Spatiales, Toulouse, where she is involved in radar altimetry. Since 2011, she has been involved in ocean calibration and validation activities, and more recently in altimetry processing over polar-regions.

Sophie Le Gac received the Ph.D. degree in Earth sciences and remote sensing techniques from the Université Pierre et Marie Curie (now Paris Sorbonne University), Paris, France, in 2010.

Since 2011, she has been involved in various radar altimetry projects, first as a Contractor for Collecte Localisation Satellites (CLS), Toulouse, from 2011 to 2015, and a Member of the radar altimetry processing team with the Centre National d'Etudes Spatiales (CNES), Toulouse. Her activities involve nadir altimetry level-1 to level-3 processing with a main focus on altimetry applications for hydrology.